

Validation of a Scaling Law for the Coronal Magnetic Field Strengths and Loop Lengths of Solar and Stellar Flares

Kosuke NAMEKATA,^{1,*} Takahito SAKAUE,¹ Kyoko WATANABE,² Ayumi ASAI³ and Kazunari SHIBATA³

¹Department of Astronomy, Kyoto University, Kitashirakawa-Oiwake-cho, Sakyo-ku, Kyoto 606-8502, JAPAN

²National Defense Academy of Japan, 1-10-20 Hashirimizu, Yokosuka, 239-8686, JAPAN

³Kwasan and Hida Observatories, Kyoto University, Yamashina, Kyoto, 607-8471, JAPAN

*namekata@kwasan.kyoto-u.ac.jp

Received 201 0; Accepted 201 0

Abstract

Shibata & Yokoyama (1999, 2002) proposed a method of estimating the coronal magnetic field strengths (B) and magnetic loop lengths (L) of solar and stellar flares, on the basis of magnetohydrodynamic simulations of the magnetic reconnection model. Using the scaling law provided by Shibata & Yokoyama (1999, 2002), B and L are obtained as functions of the emission measure ($EM = n^2 L^3$) and temperature (T) at the flare peak. Here, n is the coronal electron density of the flares. This scaling law enables the estimation of B and L for unresolved stellar flares from the observable physical quantities EM and T , which is helpful for studying stellar surface activities. To apply this scaling law to stellar flares, we discuss its validity for spatially resolved solar flares. EM and T were calculated from *GOES* soft X-ray flux data, and B and L are theoretically estimated using the scaling law. For the same flare events, B and L were also observationally estimated with images taken by *Solar Dynamics Observatory* (*SDO*)/Helioseismic and Magnetic Imager (HMI) Magnetogram and Atmospheric Imaging Assembly (AIA) 94Å pass band. As expected, a positive correlation was found between the theoretically and observationally estimated values. We interpret this result as indirect evidence that

flares are caused by magnetic reconnection. Moreover, this analysis makes us confident in the validity of applying this scaling law to stellar flares as well as solar flares.

Key words: Sun: flares — Sun: magnetic field — Sun: corona — Stars: flare

1 Introduction

Flares are the most energetic phenomena on stellar surface. It is widely believed that, during flares, magnetic energy is converted into kinetic and thermal energy through magnetic reconnection in the corona. Fast reconnection creates reconnection jets upwards and downwards from the reconnection region, and superhot components are formed on the top of the magnetic loop due to jet collisions (see e.g., Priest 1981; Shibata & Magara 2011; Shibata & Takasao 2016). The heat conduction and non-thermal particles along the magnetic field transport the thermal and non-thermal energy from the reconnection region to the foot point, and chromospheric evaporation then occurs (Neupert 1968; Hirayama 1974). Flares are observed with various wavelength ranges (Kane 1974), and several aspects of the emissions can be explained by the above flare model.

According to Feldman et al. (1995), Shimizu (1995), and Yuda et al. (1997), there is a universal correlation between the temperature (T) and emission measure (EM) among not only solar flares but also stellar flares. Shibata & Yokoyama (1999, 2002) suggested a theoretical scaling law describing this correlation. Their theory is based on two-dimensional magnetohydrodynamic simulations of magnetic reconnection with heat conduction and chromospheric evaporation from a previous study (Yokoyama & Shibata 1998), which showed that the reconnection heating ($B^2 v_A / 4\pi L$) is roughly balanced with the conduction cooling ($\kappa_0 T^{7/2} / 2L^2$) at the flare peak. They also assumed that the gas pressure (p) is comparable to the magnetic pressure ($B^2 / 8\pi$) in the evaporated plasma. Here, v_A is the Alfvén speed and κ_0 is Spitzer’s thermal conductivity. They then deduced the following scaling law:

$$B_{\text{theor}} = 50 \left(\frac{EM}{10^{48} \text{cm}^{-3}} \right)^{-1/5} \left(\frac{n_0}{10^9 \text{cm}^{-3}} \right)^{3/10} \left(\frac{T}{10^7 \text{K}} \right)^{17/10} \text{G} \quad (1)$$

$$L_{\text{theor}} = 10^9 \left(\frac{EM}{10^{48} \text{cm}^{-3}} \right)^{3/5} \left(\frac{n_0}{10^9 \text{cm}^{-3}} \right)^{-2/5} \left(\frac{T}{10^7 \text{K}} \right)^{-8/5} \text{cm} \quad (2)$$

where B_{theor} is the coronal magnetic field strength, L_{theor} is the loop length, T is the temperature and EM is the emission measure, defined as $EM = n^2 L^3$. It should be noted that n is the electron density of the evaporated plasma, whereas n_0 is the pre-flare coronal electron density around the reconnection region. It has been shown empirically that the pre-flare coronal electron density does

not vary significantly between flares and that $n_0 \sim 10^9 \text{cm}^{-3}$ (Yashiro 2000; Yashiro & Shibata 2001). The coronal magnetic field (B) and loop length (L) of a flare can therefore be calculated as functions of EM and T . We propose the following two examples as potential applications of this calculation method.

Firstly, the scaling law is important in the study of solar flares. Although it is believed that the magnetic field plays a significant role in flares, the mechanism is not completely understood, partly because of difficulties in measuring coronal magnetic fields. The scaling law is therefore helpful because it can be used to estimate coronal magnetic fields. For example, Watanabe et al. (in prep.) applied it to the study of flares associated with visible emission, called white-light flares. They statistically compared white-light flares with ‘non-white-light flares’, which emit no white light. Using this scaling law, they suggested that white-light flares tend to be associated with strong coronal magnetic fields.

Secondly, the scaling law could also be applied in stellar flare observations. Using the scaling law, the unobservable physical quantities B and L of stellar flares can be obtained from the observable physical quantities EM and T , which are measurable with soft X-ray observation (e.g., *ASCA*, *Chandra*, and *XMM-Newton*). In the past decade, many stellar and protostellar flares have been observed (e.g., Hawley & Pettersen 1991; Koyama et al. 1996; Tsuboi et al. 1998; Kowalski et al. 2010), and recently, many superflares on solar-type stars have also been detected (Maehara et al. 2012; Shibayama et al. 2013). The application of the scaling law to stellar flares has been useful in these cases. The basic structures of stellar atmospheres are considered to be very similar to that of solar atmosphere (Haisch 1989; Güdel 2002), and the flare mechanism is thought to be the same (Hayashi et al. 1996). Moreover, the estimated coronal magnetic field strength is roughly consistent with the observed values for the Sun and stars, 40-300 G (Rust & Bar 1973; Dulk 1985; Tsuneta 1996; Grosso et al. 1997). For these reasons, the scaling law can be applied to stellar flares and has in fact been used as a diagnostic tool (e.g., Yanagida et al. 2004; Grosso et al. 2004; Mitra-Kraev et al. 2005; Tsuboi et al. 2016).

To apply the scaling law of Shibata & Yokoyama (1999, 2002) to solar and stellar flares, it is necessary to test its validity. Yamamoto et al. (2002) investigated the length scales of solar flares and arcades by using the scaling law (Equation (2)), and they showed that the estimated values matched the observed values well. However, no one has tested its accuracy in calculating the coronal magnetic field strength (Equation (1)) because of the difficulty involved in measuring this parameter observationally. Aschwanden et al. (2008) commented on the necessity of statistical research on magnetic field strengths to test the scaling law. An effective test would involve investigating its validity on solar flares whose structures are spatially resolved. In this paper, we describe analysis

of 77 solar flares from the Hinode Flare Catalogue (Watanabe et al. 2012), shown in Table 1-3. The flares of this catalogue occurred in between 2011 and 2014, and were observed with *Hinode* satellite (Kosugi et al. 2007). For each flare, we present empirical estimation of the global coronal magnetic field strength of the reconnection region using *Solar Dynamics Observatory* (*SDO*) / Helioseismic and Magnetic Imager (HMI; Scherrer et al. 2012) and Atmospheric Imaging Assembly (AIA; Lemen et al. 2012) data and discuss tests of the scaling law on the coronal magnetic field strengths and the length scales of the flares. We demonstrate how to estimate these values theoretically and observationally in Section 2 and show the results of our tests of the scaling law in Section 3.

We should note here that other methods of estimating the loop length of stellar flares have been proposed. For example, Serio et al. (1991) derived a scaling law for estimating flare loop lengths from flare intensity decay time (τ_{decay}) based on the theory of flare loop cooling, $\tau_{\text{decay}} \propto L/T^{1/2}$. Reale et al. (1997) corrected this scaling law by incorporating the effect of the flare heating and also tested the validity of the scaling law using solar images. Hence, their estimation method has been widely used to estimate the stellar flare loop lengths (Reale & Micela 1998). In contrast to the scaling law of Serio et al. (1991), the application of the Shibata & Yokoyama (1999, 2002) scaling law requires measurements of the observable quantities T and EM only at the flare peak. The detailed time evolutions of these quantities are not necessary in their model, which is advantageous since it is difficult to perform high-time-resolution observations of stellar flares. We compare the two scaling laws in Appendix 1.

2 Analysis

2.1 Theoretical Estimation

Assuming that the coronal electron density does not vary significantly between flare events ($n_0 \sim 10^9 \text{cm}^{-3}$), the coronal magnetic field strength (B_{theor}) and magnetic loop length (L_{theor}) of reconnection regions can be theoretically estimated as functions of T and EM , using Equations (1) and (2). As illustrated in Figure 1, reconnection regions are defined in this paper as global coronae in which magnetic energy is converted into kinetic and thermal energy, and flaring regions are defined as flaring coronal regions with bright soft X-ray or EUV emission. T and EM were calculated using a filter ratio method with *GOES* soft X-ray fluxes. In this method, we used the program *goes_chianti_tem* that is incorporated into the Solar SoftWare (SSW) package in IDL. We calculated the physical quantities required when EM was at a maximum, as the T value calculated by the filter ratio method is weighted by EM .

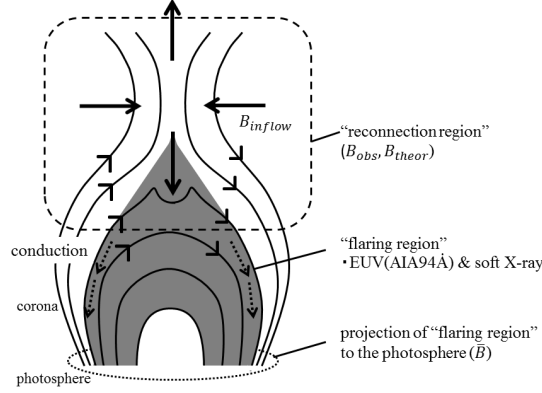


Fig. 1. Simple illustration of a magnetic reconnection model of flares. In this paper, reconnection regions are defined as global coronae in which magnetic energy is converted into kinetic and thermal energy, and flaring regions are defined as flaring coronal regions with bright soft X-ray or EUV emission. To estimate the coronal magnetic field strength of the reconnection region (B_{theor}), we measured the photospheric magnetic field strength under the flaring region (\overline{B} ; inside the dotted line).

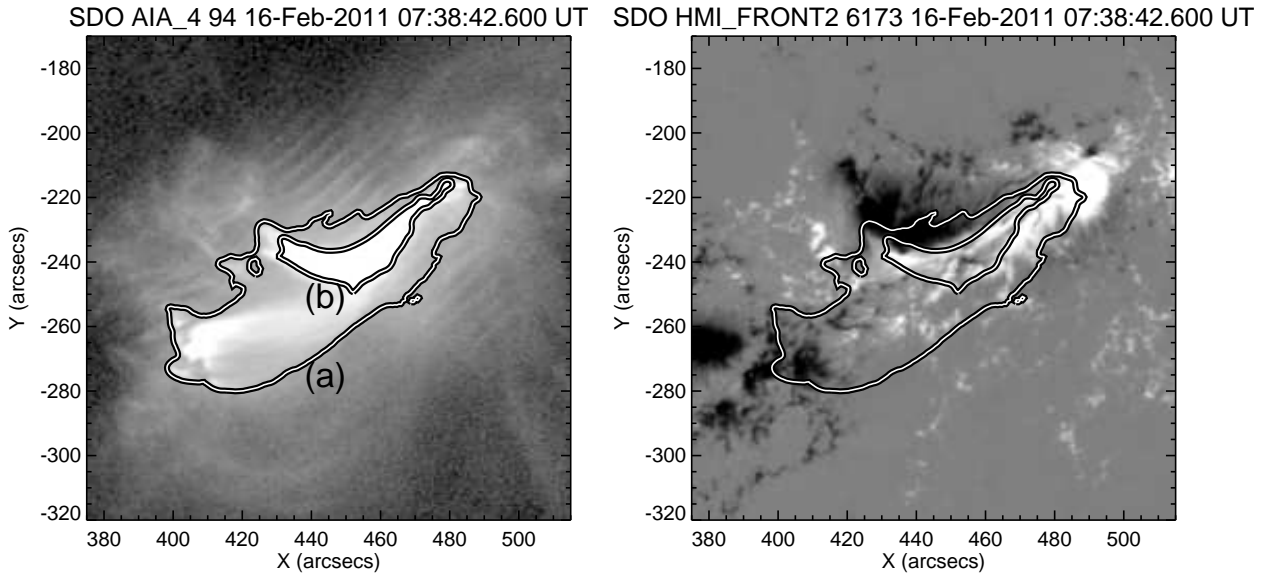


Fig. 2. Left: EUV image obtained with *SDO/AIA* 94Å on February 14, 2011. The image was observed at the peak time of *GOES* soft X-ray, and we regarded flaring regions as regions with the intensities $>30 \text{ DN s}^{-1}$ (a; outer contour) and $>500 \text{ DN s}^{-1}$ (b; inner contour) in the image of *AIA* 94Å. Right: Image of the line-of-sight photospheric magnetic field obtained with *SDO/HMI* Magnetgram at the same time as the left image. As illustrated in Figure 1, we measured the mean of the absolute value of magnetic field strength (\overline{B}) in the flaring region, and calculated the coronal magnetic field of the reconnection regions (B_{obs}) using the empirical relation $B_{\text{obs}} = \overline{B}/3$.

2.2 Observational Estimation

Using an empirical relation, we observationally estimated the global coronal magnetic field strength where the magnetic energy was released. The analysis method was as follows. First, we defined the flaring regions in two different ways for comparison. The contours portrayed in the left of Figure

2 show the flaring regions, defined as (a) regions with intensities $>30 \text{ DN s}^{-1}$ and (b) regions with intensities $>500 \text{ DN s}^{-1}$ in the images taken with *SDO/AIA* 94Å at the flare peak. Second, the mean of the absolute values of the photospheric magnetic field strength inside the projections of the flaring regions to the photosphere (\overline{B}) were given by *SDO/HMI* Magnetogram (see, Figure 1 and the right panel of Figure 2). The HMI images of very strong magnetic field regions could sometimes become saturated, so we replaced the saturated regions with the averages of the surrounding values. It is empirically known that the coronal magnetic field strengths of reconnection regions, B_{obs} , are smaller by factors of ~ 3 than photospheric ones, \overline{B} (e.g., Isobe et al. 2005; Narukage & Shibata 2006), and we therefore observationally estimated the coronal magnetic field as $B_{\text{obs}} = \overline{B}/3$.

Although the coronal magnetic field strength can be extrapolated in the other ways (e.g., using a potential field or a force free field), we did not use these methods. It is not necessary to concern ourselves with measuring the coronal magnetic field strength exactly, since the scaling law itself still involves some error. In the analysis discussed in this report, we examined whether there was a positive correlation between the theoretically estimated magnetic field strength B_{theor} and the roughly measured one B_{obs} . In addition, we defined the observed magnetic loop length scale L_{obs} as the square root of the area of the flaring region for simplicity and examined the relation between L_{theor} and L_{obs} .

3 Testing

3.1 Coronal Magnetic Field of the Flaring Region

We compared the theoretically estimated coronal magnetic field strength calculated using the scaling law (B_{theor}) with the observationally estimated one described in Section 2.2 (B_{obs}). Figure 3 shows comparisons between B_{theor} and B_{obs} . The left and right figures correspond to the case (a) and (b), respectively. The squares and crosses indicate the flares around the disk center and the solar limb, respectively. The disk center is defined as the area whose radial distance from the solar center is less than 600 arcsec (solar radius ~ 1000 arcsec). As expected, there is a positive correlation between B_{theor} and B_{obs} , regardless of the definitions of the flaring regions.

We obtained this positive correlation using only simple analysis, which supports the validity of the initial assumption that flares are caused by magnetic reconnection, as well as supporting the application to stellar flares. The scaling law makes it possible to estimate the magnetic field strengths of unresolved stellar flares without high-resolution spectroscopy or high-time-resolution photometry, as mentioned in Section 1. Such a simple method would be helpful for studying stellar flares, especially in large-sky surveys of nearby active flare stars. Statistical studies of stellar magnetic field strengths calculated using this scaling law may provide clues to understanding stellar activity.

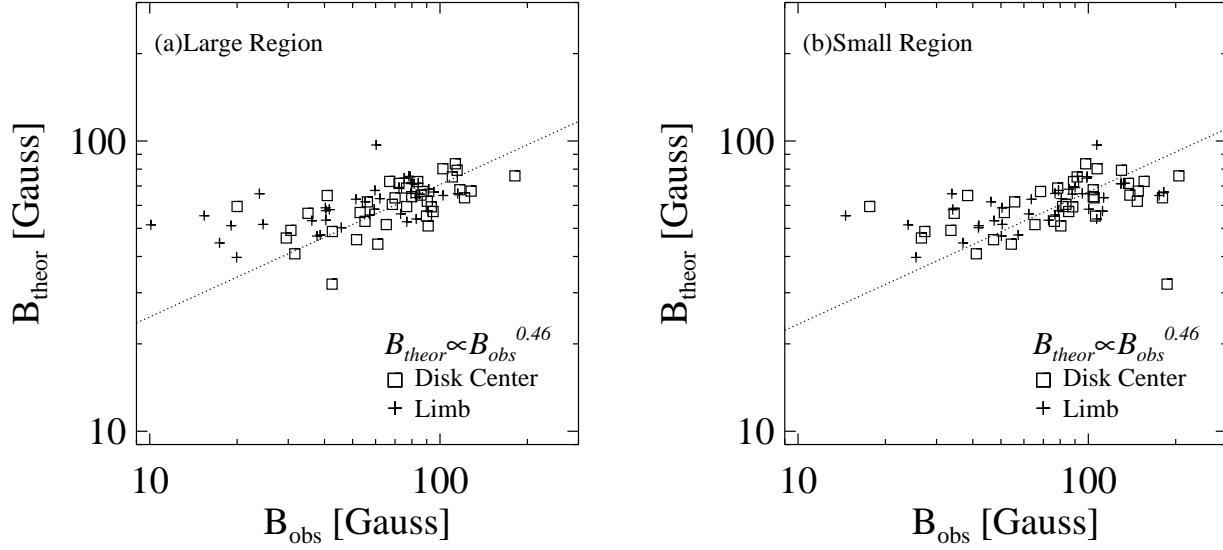


Fig. 3. Comparisons between the measured coronal magnetic field strength (based on *SDO/HMI*) and the theoretically calculated one (based on the theory of Shibata & Yokoyama (2002) and *GOES* X-ray data). The left figure shows case (a), where flaring regions are large and are defined by a 30 DN s^{-1} contour, and the right is case (b), where flaring regions are small and are defined by 500 DN s^{-1} . Squares indicate flares with radial distances from the solar center of less than 600 arcsec, and crosses indicate those at distances greater than 600 arcsec. The dotted line is a fit for only the flares in the disk center, which was obtained using an ordinary least square bisector, and the power law index is 0.46 for both lines.

As demonstrated in Figure 3, B_{theor} is not in proportional to B_{obs} , although it should be proportional if the scaling law is correct. There are two possible reasons for this discrepancy. The first is related to the problem of the filter ratio method. The filter ratio method for *GOES* incorporated into SSWIDL tends to estimate temperatures closer to 1 MK, which may have resulted in the narrow range of the theoretically estimated values as shown in Figure 3. The second reason is the method of extrapolating B_{obs} , which was done using the simple empirical relation $B_{\text{obs}} = \overline{B}/3$. Moreover, the ‘photospheric’ magnetic field strength was measured inside the regions defined by the ‘coronal’ EUV brightness (*SDO/AIA* 94Å), making the estimated magnetic field strength smaller, especially for flares in the limb. The flares in the limb and disk center are plotted individually in Figure 3, which shows that the observationally estimated values for flares in the limb tend to differ significantly from the theoretically estimated values. By an ordinary least-squares bisector fitting (Isobe et al. 1990), the power law index was calculated to be ~ 0.37 for all of the flares and ~ 0.46 for the flares in the disk center in case (a), and ~ 0.39 for all of the flares and ~ 0.46 for the flares in the disk center in case (b).

3.2 Flare Loop Length

Yamamoto et al. (2002) previously tested the scaling law for C-, M- and X-class flares and arcades and reported a strong correlation between L_{theor} and L_{obs} . They calculated T and EM using a filter

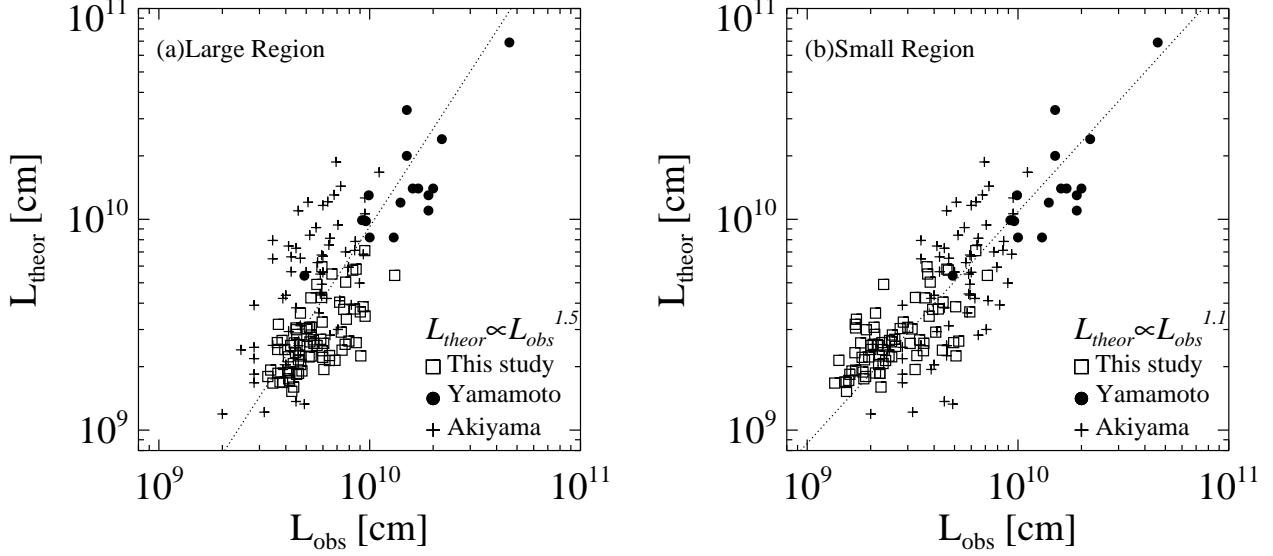


Fig. 4. Comparisons between the observationally estimated length scales (L_{obs}) and the theoretically estimated ones (L_{theor}) from Shibata & Yokoyama (2002). Squares correspond to flares listed in this paper, crosses indicate flares taken from Akiyama et al. (2001), and filled circles show arcades from Yamamoto et al. (2002). The left figure is case (a) and the right is case (b). L_{obs} matches L_{theor} well in case (b) and the power law index is ~ 1.1 .

ratio method with *Yohkoh*'s soft X-ray images, and the length scales of the flares and arcades were defined as the square root of the area of the flaring regions and the height of the arcades, respectively. Considering applications to the stellar flares, we examined the validity of the scaling law using X-ray fluxes measured with *GOES* satellites, which is unable to resolve the structures.

As described in Section 2.2, the loop length scales of the flares, L_{obs} , were measured as the square roots of the areas of the flaring regions with bright EUV emission in cases (a) and (b). Figure 4 shows comparisons between L_{obs} and L_{theor} . The open squares correspond to the M- and X-class flares discussed in this paper. The crosses indicate the C-, M- and X-class flare data measured by Akiyama et al. (2001) and the filled circles show the arcades measured by Yamamoto et al. (2002). In case (a), in which the measured area is defined by a lower threshold (30 DN s^{-1}), the measured loop length scale L_{obs} tends to be larger than the theoretically estimated L_{theor} . On the other hand, we can see that L_{theor} roughly matches L_{obs} with $\sigma \sim 0.56$, in case (b), where the measured area consists of bright flaring components. The power law index is ~ 0.89 for our data and ~ 1.10 for all of the data, including that of Akiyama et al. (2001) and Yamamoto et al. (2002).

These results show that the scaling law can be used to obtain accurate estimations of the magnetic loop lengths of flares. In combination with photometry to estimate stellar spot sizes, this method would be helpful for constraining the magnetic field structures of unresolved stellar flares.

4 Summary and Discussion

Shibata & Yokoyama (1999, 2002) suggested a method of estimating the coronal magnetic field strengths and magnetic loop length scales of solar and stellar flares from observations with an instrument that is unable to resolve their structure. In this paper, we described tests of the scaling law on spatially resolved solar flares with *GOES* and *SDO/HMI* and *AIA* data and found a positive correlation between the theoretically estimated physical quantities obtained with the scaling law and the observationally estimated values. We consider this analysis to support the theory of magnetic reconnection indirectly and to enable the application of the scaling law in the two scenarios described in Section 1.

First, the scaling law provides an important suggestion regarding the unsolved mechanism of white-light flares by showing that the coronal magnetic fields of flares with white-light emission tend to be stronger than that of flares with no white light (Watanabe et al. in prep). This fact can be used to constrain white-light flare models, such as the model in which the main source of the flare optical continuum is the chromospheric condensation formed in the response of the chromosphere to flare heating (Fisher et al. 1985; Abbett & Hawley 1999). The reconnection with the strong magnetic field can lead to strong white-light emission.

Moreover, this analysis enables the application of the scaling law to the unresolved stellar flares and the determination of unobservable physical quantities. We should take into account the following two features regarding the application of the scaling law to stellar flares. Firstly, it is necessary to measure the maximum T and EM values of the flares as described in Section 2. In stellar flare observations, T does not vary significantly during flares, regardless of the time cadence of the observations, while the maximum EM may be reduced by a factor of 2-3 with long-exposure-time observations (e.g., Tsuboi et al. 2000). This results in an increase in the estimated loop length by a factor of 1.5-1.9 (see, Equation (2)) and does not affect the estimation. Secondly, it may be necessary to measure the pre-flare coronal density n_0 , especially in the case of stellar flares, because n_0 may be higher by an order of magnitude for active stellar atmospheres and the estimated loop length can then be lower by a factor of ~ 3 .

Finally, we emphasize the usefulness of this method for stellar observations as follows:

1. It can be used to estimate unobservable physical quantities theoretically, such as the coronal magnetic field strengths and loop lengths of unresolved stellar flares.
2. The application of the scaling law requires only photometric observations with an instrument that has a high sensitivity and moderate spectral resolution. Such a simple method would be useful in a large-sky survey of nearby active stars.

3. Additionally, the scaling law requires measurements of observed quantities only at the flare peak, while other scaling laws require time-evolution data of the rising or decay phases of flares. As we noted, the estimation for the scaling law presented does not require high-time-cadence observations, which is advantageous, especially in the case of impulsive flares.

Acknowledgement: We acknowledge with thanks Y. Notsu and S. Takasao for their contribution of fruitful comments on our work. We are grateful to the *SDO*/AIA and HMI teams. *SDO* is part of NASAs Living with a Star Program. This work was partly carried out by using the Hinode Flare Catalogue (http://st4a.stelab.nagoya-u.ac.jp/hinode_flare/), which is maintained by ISAS/JAXA and the Institute for Space-Earth Environmental Research, Nagoya University. *Hinode* is a Japanese mission developed and launched by ISAS/JAXA with NAOJ as a domestic partner and NASA and STFC (UK) as international partners. This work was supported by JSPS KAKENHI Grant Numbers JP16H03955, JP15K17772, JP15K17622 and JP16H01187. The authors would like to thank Enago (www.enago.jp) for English language review.

Appendix 1 Comparison with Reale et al. (1997)

We examined the validity of a scaling law proposed by Reale et al. (1997) by applying it to the same flare catalogue used in this paper. As explained in Section 1, Serio et al. (1991) first derived this scaling law for a flare loop in the decay phase. By incorporating the effect of heating during the decay phase into the scaling law, Reale et al. (1997) corrected it as follows:

$$L = \frac{\tau_{LC}\sqrt{T}}{\alpha F(\zeta)} \quad (\text{A1})$$

where τ_{LC} is a light curve decay time, α is $3.7 \times 10^{-4} \text{cm}^{-1} \text{sK}^{1/2}$, ζ is the slope in the $\sqrt{EM}-T$ diagram in the decay phase, and $F(\zeta)$ is the correction function:

$$F(\zeta) = \frac{c_a}{\zeta/\zeta_a - 1} + q_a \quad (\text{A2})$$

where $c_a = 5.4 \pm 1.5$, $\zeta_a = 0.25 \pm 0.04$, and $q_a = 0.52 \pm 0.16$. In this study, we used *GOES* soft X-ray fluxes to measure T , τ_{LC} and ζ . As described by Reale et al. (1997), τ_{LC} is defined as the time taken for the *GOES* count to decrease by $1/e$ from its maximum value. The slope ζ of the $\sqrt{EM}-T$ diagram was measured with a linear regression method, and the measured ranges were determined by eye as the ranges in which the slopes appeared straight in the diagrams. The measured values are listed in Table 1. We selected events that met the following condition:

1. They were listed in this paper and Reale et al. (1997).
2. They satisfied the conditions in which the Reale et al. (1997) scaling law holds.

3. $\zeta \leq 1.2$ (a range consistent with Reale et al. (1997)).

We then compared the estimation methods of Shibata & Yokoyama (1999, 2002) with that of Reale et al. (1997). Note that the ζ values in many flares were unmeasurable (see Table 1).

Figures 5 and 6 show comparisons of the two scaling laws. In this analysis, we measured the flaring loop lengths in two ways. The loop length in Figure 5 is defined as the square root of the area of the flaring regions measured with *SDO/AIA* 94Å, and the loop length in Figure 6 is the distance between two ribbons measured with *SDO/AIA* 1600Å. The left and right panels in each figure show the results of Shibata & Yokoyama (1999, 2002) and Reale et al. (1997). The unfilled squares correspond to the flares listed in this paper, and the circles indicate those selected by Reale et al. (1997) to test their scaling law. The filled circles are events for which the flare loops were clearly measured, and the unfilled ones are events for which flare loops were too complex to measure. The estimated values obtained with both scaling laws are consistent with the true values, except for in some individual events. In the right panels of Figure 5 and 6, the loop length estimates from Reale et al. (1997) are scattered. This scattering is present because, while Reale et al. (1997) measured ζ using the spatially resolved images taken with *Yohkoh*, it is difficult to measure well-defined ζ values with *GOES* satellite, which observes the entire solar surface. The overall solar emission measure $EM_s \sim 10^{48-49} \text{cm}^{-3}$ is comparable to the flare value of $EM \sim 10^{49} \text{cm}^{-3}$, which makes it difficult to measure ζ precisely, especially in observations of flares on solar-type stars (G stars). Another reason is that there is a difference between the instruments used by Reale et al. (1997) and those used by this study. Reale et al. (1997) used the light curves with *Yohkoh* Al 11.4 μm filter band, which is sensitive to a few mega-Kelvin, while we used *GOES* 1-8Å pass band, which is sensitive to a few tens of mega-Kelvin.

Finally, we compared the practicality of the two scaling laws. Reale et al. (1997)’s scaling law requires time-evolution data for the flares to estimate physical quantities, while that of Shibata & Yokoyama (1999, 2002) does not require high-time-cadence observations, as noted in Section 4. This is a significant advantage because it is difficult to observe stellar flares with high time cadence. Moreover, methods that use decay or rising phases introduce additional uncertainties, since the soft X-ray light curves of flares are superpositions of light curves of several flaring loops that reconnect one after another. In terms of application to stellar observations, we consider the scaling law of Shibata & Yokoyama (2002) to be more useful for estimating the physical parameters of unresolved stellar flares.

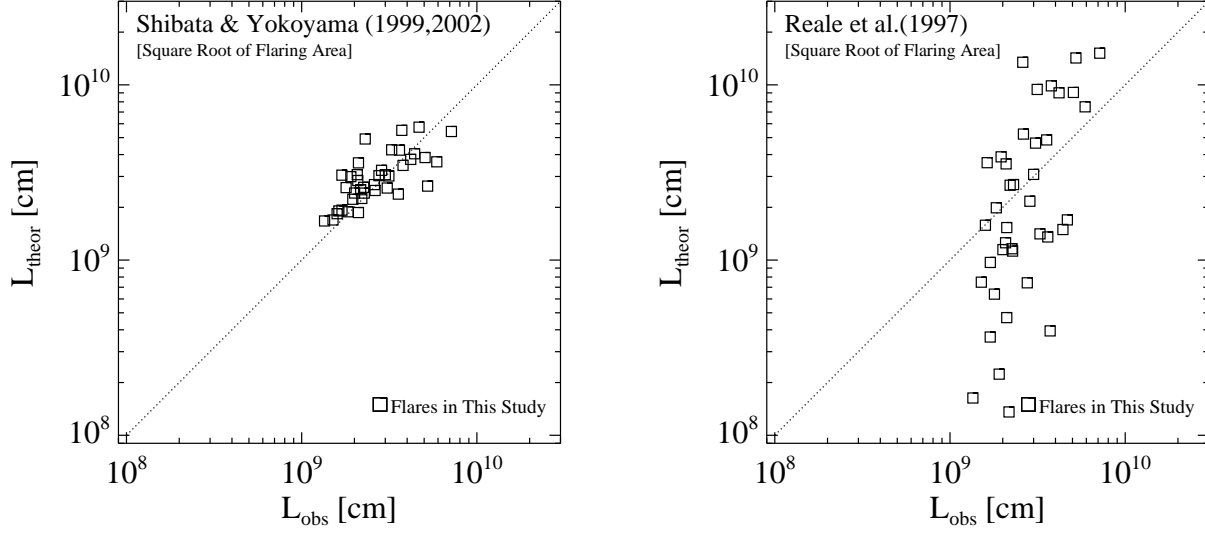


Fig. 5. Left and right figures show comparisons between the observationally measured and theoretically estimated loop lengths using the scaling law of Shibata & Yokoyama (2002) and Reale et al. (1997), respectively. The loop lengths were measured as the square roots of the flaring regions defined by 500 DN s^{-1} (b; inner contour) of the brightness from AIA 94Å as described in Section 2.

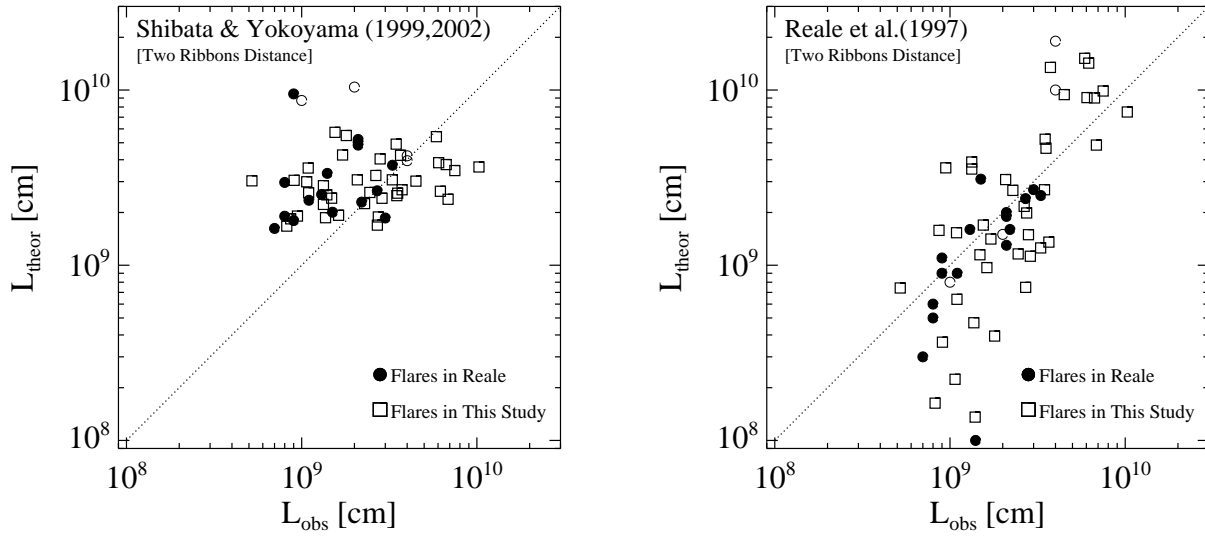


Fig. 6. Left and right figures show comparisons between the observationally measured and theoretically estimated loop lengths using the scaling law of Shibata & Yokoyama (2002) and Reale et al. (1997), respectively. The loop lengths were measured as the distance of two ribbons in images taken by AIA 1600Å. Since it was difficult to measure the distances between the two ribbons at the flare peaks due to the saturation of the images, we analyzed the images 5 min after the flare peaks. The distances were measured by eye between the brightest points of the flare ribbons.

References

- Akiyama, S. 2001, Ph.D. thesis, Grad. Univ. Adv. Study, NAOJ
- Aschwanden, M. J., Stern, R. A. 2008, *ApJ*, 672, 659-673
- Dulk, G. A. 1985, *ARA&A*, 23, 169
- Feldman, U., Laming, J. M., & Doschek, G. A. 1995, *ApJL*, 451, L79
- Fisher, G. H., Canfield, R. C., & McClymont, A. N. 1985, *ApJ*, 289, 414
- Abbett, W. P., & Hawley, S. L. 1999, *ApJ*, 521, 906
- Grosso, N., Montmerle, T., Feigelson, E. D., et al. 1997, *Nature*, 387, 56
- Grosso, N., Montmerle, T., Feigelson, E. D., & Forbes, T. G. 2004, *A&A*, 419, 653
- Güdel, M. 2002, *ARA&A*, 40, 217
- Haisch, B. M. 1989, *Sol. Phys.*, 121, 3
- Hawley, S. L., & Pettersen, B. R. 1991, *ApJ*, 378, 725
- Hayashi, M. R., Shibata, K., & Matsumoto, R. 1996, *ApJL*, 468, L37
- Hirayama, T. 1974, *Sol. Phys.*, 34, 323
- Isobe, T., Feigelson, E. D., Akritas, M. G., & Babu, G. J. 1990, *ApJ*, 364, 104
- Isobe, H., Takasaki, H., & Shibata, K. 2005, *ApJ*, 632, 1184
- Kane, S. R. 1974, in *IAU Symposium, Vol. 57, Coronal Disturbances*, ed. G. A. Newkirk, 105141
- Kosugi, T., Matsuzaki, K., Sakao, T., et al. 2007, *Sol. Phys.*, 243, 3
- Kowalski, A. F., Hawley, S. L., Holtzman, J. A., Wisniewski, J. P., & Hilton, E. J. 2010, *ApJL*, 714, L98
- Koyama, K., Hamaguchi, K., Ueno, S., Kobayashi, N., & Feigelson, E. D. 1996, *PASJ*, 48, L87
- Lemen, J. R., Title, A. M., Akin, D. J., et al. 2012, *Sol. Phys.*, 275, 17
- Maehara, H., Shibayama, T., Notsu, S., et al. 2012, *Nature*, 485, 478
- Mitra-Kraev, U., Harra, L. K., Williams, D. R., & Kraev, E. 2005, *A&A*, 436, 1041
- Narukage, N., & Shibata, K. 2006, *ApJ*, 637, 1122
- Neupert, W. M. 1968, *ApJL*, 153, L59
- Priest, E. R. 1981, *Solar Flare Magnetohydrodynamics* New York; Gordon and Breach Science Publishers)
- Reale, F., Betta, R., Peres, G., Serio, S., & McTiernan, J. 1997, *A&A*, 325, 782
- Reale, F., & Micela, G. 1998, *A&A*, 334, 1028
- Rust, D. M., & Bar, V. 1973, *Sol. Phys.*, 33, 445
- Scherrer, P. H., Schou, J., Bush, R. I., et al. 2012, *Sol. Phys.*, 275, 207
- Serio, S., Reale, F., Jakimiec, J., Sylwester, B., & Sylwester, J. 1991, *A&A*, 241, 197
- Shibata, K., & Takasao, S. 2016, in “Magnetic Reconnection”, Gonzalez, W., & Parker, E. N. (eds.), p.373
(2016: Springer International Publishing Switzerland)

Shibata, K., & Yokoyama, T. 1999, ApJL, 526, L49
 Shibata, K., & Yokoyama, T. 2002, ApJ, 577, 422
 Shibata, K., & Magara, T. 2011, Living Reviews in Solar Physics, 8, 6
 Shibayama, T., Maehara, H., Notsu, S., et al. 2013, ApJS, 209, 5
 Shimizu, T. 1995, PASJ, 47, 251
 Tsuboi, Y., Koyama, K., Murakami, H., et al. 1998, ApJ, 503, 894
 Tsuboi, Y., Imanishi, K., Koyama, K., Grosso, N., & Montmerle, T. 2000, ApJ, 532, 1089
 Tsuboi, Y., Yamazaki, K., Sugawara, Y., et al. 2016, PASJ, 68, 90
 Tsuneta, S. 1996, ApJ, 456, 840
 Watanabe, K., Masuda, S., & Segawa, T. 2012, Sol. Phys., 279, 317
 Watanabe, K, in preparation
 Yamamoto, T. T., Shiota, D., Sakajiri, T., et al. 2002, ApJL, 579, L45
 Yanagida, T., Ezoe, Y.-I., & Makishima, K. 2004, PASJ, 56, 813
 Yashiro, S. 2000, Ph.D. thesis, Univ. Tokyo
 Yashiro, S., & Shibata, K. 2001, ApJL, 550, L113
 Yokoyama, T., & Shibata, K. 1998, ApJL, 494, L113
 Yuda, S., Hiei, E., Takahashi, M., & Watanabe, T. 1997, PASJ, 49, 115

Table 1. Physical parameters of flares.

peak time	GOES class	Loc.* [deg]	T_6^\dagger [K]	EM_{48}^\ddagger [cm ⁻³]	B_{theor}^\S [G]	$B_{\text{obs}}(a)^\parallel$ [G]	$B_{\text{obs}}(b)^\#$ [G]	L_{theor}^\S [10 ⁹ cm]	$L_{\text{obs}}(a)^\parallel$ [10 ⁹ cm]	$L_{\text{obs}}(b)^\#$ [10 ⁹ cm]	L_{Reale}^{**} [10 ⁹ cm]	$\tau_{\text{SXR}}^{\dagger\dagger}$ [sec]	$\zeta^{\ddagger\ddagger}$
2011/02/14-17:26	M2.2	S20W04	15.5	1.2	63.7	70.0	104.7	2.2	5.2	2.0	3.9	770	1.04
2011/02/15-01:56	X2.2	S20W10	19.6	10.3	62.0	90.4	147.5	5.5	6.6	3.7	0.4	747	0.30
2011/02/16-07:44	M1.1	S19W29	14.3	0.6	63.7	121.5	180.1	1.7	3.9	1.5	—	—	—
2011/02/18-10:11	M6.6	S21W55	18.6	3.4	71.2	81.5	129.4	3.1	4.5	1.7	0.4	233	0.42
2011/02/18-13:03	M1.4	S21W55	15.7	0.8	71.3	79.7	129.9	1.7	3.5	1.4	0.2	274	0.32
2011/09/23-22:15	M1.6	N12E56	12.7	1.0	47.4	38.7	57.3	2.7	5.9	2.6	13.5	3209	0.97
2011/11/02-22:01	M4.3	N20E77	17.2	2.1	68.2	91.5	85.7	2.6	5.2	2.5	—	1384	—
2011/11/03-11:11	M2.5	N20E70	15.9	1.3	65.6	85.0	88.1	2.2	4.7	2.2	2.7	917	0.64
2011/11/03-20:27	X1.9	N21E64	21.5	8.7	75.5	78.1	91.8	4.3	5.9	3.3	1.4	407	0.66
2011/11/05-03:31	M3.7	N20E47	15.8	1.5	63.8	82.6	112.9	2.4	7.4	4.4	—	2209	—
2011/11/05-20:38	M1.8	N21E37	17.0	0.9	79.3	114.5	130.1	1.6	4.4	2.2	—	1427	—
2011/12/31-13:15	M2.4	S25E46	17.0	1.2	74.5	75.3	98.8	1.9	3.4	1.7	1.0	352	0.61
2011/12/31-16:26	M1.5	S25E42	15.1	0.9	65.9	79.5	76.8	1.9	3.7	2.2	—	636	—
2012/01/17-04:53	M1.0	N18E53	14.0	0.6	61.7	55.2	46.2	1.7	4.2	1.6	—	1429	—
2012/01/18-19:12	M1.7	N17E32	14.4	1.0	59.4	76.8	81.5	2.2	4.6	1.9	—	1476	—
2012/01/27-18:37	X1.7	N33W85	15.9	9.0	44.6	17.4	37.0	7.1	9.5	6.3	—	1480	—
2012/03/05-04:05	X1.1	N19E58	18.2	5.0	63.0	51.3	63.6	4.0	7.2	4.4	1.5	2785	0.31
2012/03/06-12:41	M2.1	N21E40	16.0	1.1	67.9	117.1	104.0	2.0	4.7	2.2	—	1105	—
2012/03/06-21:11	M1.3	N16E30	16.1	0.7	75.8	181.2	205.1	1.5	4.3	1.5	—	—	—
2012/05/07-14:31	M1.9	S20W49	14.0	1.0	55.3	15.4	14.6	2.4	6.0	3.6	4.8	1777	0.66
2012/05/09-12:32	M4.7	N13E31	17.8	2.3	71.4	72.2	137.5	2.6	4.4	1.8	0.6	260	0.56
2012/05/09-14:08	M1.8	N06E22	13.4	1.1	51.0	91.1	80.4	2.6	3.6	2.3	1.2	374	0.68
2012/05/09-21:05	M4.1	N12E26	17.7	2.0	72.5	83.8	88.9	2.4	3.7	2.0	1.1	346	0.66
2012/05/10-20:26	M1.7	N12E12	15.7	0.9	68.8	76.7	78.4	1.9	4.1	2.1	0.5	616	0.35
2012/06/13-13:17	M1.2	S16E18	13.5	0.7	56.7	53.1	51.4	1.9	6.1	3.2	—	—	—
2012/07/05-03:36	M4.7	S18W29	18.0	2.3	72.6	67.1	155.7	2.6	7.6	2.1	—	249	—
2012/07/05-21:45	M1.6	S12W46	13.4	1.0	51.6	24.6	50.5	2.5	5.6	2.0	—	—	—
2012/07/06-01:40	M2.9	S18W41	16.3	1.5	66.7	95.2	181.8	2.3	4.5	1.7	—	176	—
2012/07/06-08:23	M1.5	S17W40	15.0	0.8	64.9	102.5	175.4	1.9	4.2	1.8	2.0	727	0.64
2012/07/06-23:08	X1.1	S13W59	16.6	5.5	53.1	36.2	47.4	4.9	5.6	2.3	2.7	542	0.86
2012/07/08-12:09	M1.4	S21W69	15.8	0.8	71.5	84.2	133.6	1.7	3.8	1.5	0.7	274	0.62
2012/07/12-16:49	X1.4	S13W03	20.5	3.4	83.5	112.9	98.0	2.6	8.0	5.2	14.2	3536	0.77
2012/07/14-04:58	M1.0	S22W36	9.7	0.7	32.1	42.5	186.8	3.4	7.8	1.7	—	—	—
2012/10/23-03:17	X1.8	S13E58	24.2	6.7	96.9	60.3	106.9	3.0	5.0	2.8	0.7	303	0.51
2013/05/02-05:10	M1.1	N10W26	12.4	0.7	49.2	30.6	33.6	2.2	4.1	2.5	—	651	—
2013/05/03-16:55	M1.3	N10W38	12.3	0.8	46.3	29.5	26.6	2.6	6.1	3.6	—	—	—
2013/05/15-01:40	X1.2	N12E64	15.8	6.6	47.1	37.7	50.2	6.0	5.9	3.7	—	909	—

Table 2. Physical parameter of flares (continued).

peak time	GOES class	Loc.* [deg]	T_6^\dagger [K]	EM_{48}^\ddagger [cm ⁻³]	B_{theor}^\S [G]	$B_{\text{obs}}(a)^\parallel$ [G]	$B_{\text{obs}}(b)^\#$ [G]	L_{theor}^\S [10 ⁹ cm]	$L_{\text{obs}}(a)^\parallel$ [10 ⁹ cm]	$L_{\text{obs}}(b)^\#$ [10 ⁹ cm]	L_{Reale}^{**} [10 ⁹ cm]	$\tau_{\text{SXR}}^{\dagger\dagger}$ [sec]	$\zeta^{\ddagger\ddagger}$
2013/06/07-22:49	M5.9	S32W89	17.4	2.9	65.8	23.9	33.9	3.1	5.3	3.0	3.1	1204	0.58
2013/08/17-18:24	M3.3	S07W30	16.4	1.7	65.1	86.0	139.1	2.5	4.7	2.2	—	—	—
2013/10/22-00:22	M1.0	N06E17	13.6	0.6	59.3	93.3	88.4	1.8	4.1	1.9	—	571	—
2013/10/26-19:31	M3.1	S09E81	14.2	1.7	51.1	19.1	41.9	3.2	3.7	1.7	—	380	—
2013/10/28-15:01	M2.7	S08E28	15.3	1.5	60.5	68.5	83.7	2.5	4.2	2.2	0.1	141	0.37
2013/10/28-15:15	M4.4	S06E28	13.6	2.5	44.1	61.1	54.3	4.2	5.3	3.6	1.4	1030	0.42
2013/12/07-07:29	M1.2	S16W49	11.3	0.9	39.7	19.9	25.5	3.0	5.0	3.1	9.4	2289	0.97
2013/12/22-08:11	M1.9	S20W49	15.9	1.0	69.2	72.2	90.1	1.9	4.8	1.6	3.6	722	0.99
2013/12/22-15:12	M3.3	S19W56	15.4	1.8	58.2	59.4	100.3	2.8	4.5	2.1	3.5	739	1.02
2013/12/23-09:06	M1.6	S17W63	15.4	0.9	67.5	59.7	78.9	1.8	4.5	1.6	1.6	286	1.18
2013/12/31-21:58	M6.4	S16W35	17.4	3.1	64.3	79.9	104.0	3.3	6.0	2.9	2.2	1593	0.42
2014/01/01-18:52	M9.9	S14W47	15.9	5.1	50.3	45.7	41.8	5.0	7.7	3.8	—	1007	—
2014/01/04-10:25	M1.3	S05E48	13.6	0.8	56.1	73.2	62.3	2.1	4.3	2.3	—	—	—
2014/01/04-19:46	M4.0	S11E34	15.2	1.5	59.5	20.0	17.7	2.6	8.6	5.0	—	3219	—
2014/02/14-02:57	M2.3	S12W25	14.6	1.3	57.2	94.7	85.6	2.5	5.0	2.6	5.2	1198	0.94
2014/02/14-12:40	M1.6	S15W36	13.9	0.9	56.3	35.1	34.5	2.2	6.0	1.8	—	415	—
2014/03/13-19:19	M1.2	N15W87	12.9	0.8	51.4	10.1	24.0	2.3	6.5	3.3	—	1105	—
2014/06/12-22:16	M3.1	S20W55	14.2	1.0	57.5	40.5	79.0	2.2	9.1	5.1	—	3536	—
2014/06/16-00:01	M1.0	S19E08	11.1	0.7	40.9	31.6	41.1	2.7	3.8	2.5	—	2019	—
2014/08/01-18:03	M1.5	S10E11	12.3	0.9	45.7	51.6	47.1	2.7	5.4	3.4	—	3260	—
2014/10/21-13:38	M1.2	S14E35	14.8	0.8	64.9	40.9	38.4	1.8	3.3	1.9	—	129	—
2014/10/22-01:59	M8.7	S13E21	18.4	4.0	67.2	128.0	148.6	3.5	9.5	3.8	9.9	2297	0.84
2014/10/22-14:06	X1.6	S14E13	20.5	5.9	75.2	110.3	91.5	3.6	9.0	5.9	7.5	1710	0.77
2014/10/24-21:15	X3.1	S16W21	19.4	9.8	61.7	56.2	55.8	5.4	13.1	7.2	15.2	2646	1.00
2014/10/25-17:08	X1.0	S10W22	18.7	4.8	67.0	87.5	68.5	3.7	7.5	3.9	—	—	—
2014/10/26-10:56	X2.0	S18W40	21.9	7.3	80.2	102.3	107.2	3.8	8.5	4.2	9.0	1683	0.93
2014/10/26-20:21	M2.4	S15W45	15.7	1.2	65.9	115.1	95.4	2.1	6.4	2.4	—	—	—
2014/10/27-14:23	X2.0	S17W52	20.9	6.7	75.4	79.0	99.1	3.8	9.3	5.1	9.1	1763	0.92
2014/10/28-02:42	M3.4	S14W61	15.3	1.8	57.3	91.0	111.9	2.9	7.3	4.1	—	—	—
2014/10/29-10:01	M1.2	S18W77	13.0	0.7	52.7	76.9	—	2.1	6.8	1.4	—	—	—
2014/11/05-09:47	M7.9	N20E68	17.6	3.8	63.3	62.1	80.8	3.6	4.7	2.1	1.5	679	0.50
2014/11/05-19:44	M2.9	N17E65	15.1	1.4	58.9	40.3	50.4	2.6	5.4	3.1	4.7	2525	0.50
2014/11/07-02:44	M2.7	N17E50	14.3	1.5	53.9	82.8	106.8	2.8	5.3	2.5	—	—	—
2014/11/07-10:20	M1.0	N15E43	13.1	0.6	55.6	57.3	76.8	1.9	4.6	2.2	—	954	—
2014/11/07-17:26	X1.6	N14E36	17.3	7.9	52.9	55.1	76.4	5.7	8.3	4.7	1.7	798	0.52
2014/11/15-12:03	M3.2	S09E63	14.6	1.8	53.4	40.4	72.9	3.1	5.2	2.1	1.3	559	0.53
2014/11/15-20:46	M3.7	S13E63	15.5	2.0	58.0	41.6	34.1	3.0	4.5	1.9	0.2	276	0.35

Table 3. Physical parameter of flares (continued).

peak time	<i>GOES</i> class	Loc.* [deg]	T_6 [†] [K]	EM_{48} [‡] [cm ⁻³]	B_{theor} [§] [G]	$B_{\text{obs}}(a)$ [G]	$B_{\text{obs}}(b)$ [#] [G]	L_{theor} [§] [10 ⁹ cm]	$L_{\text{obs}}(a)$ [10 ⁹ cm]	$L_{\text{obs}}(b)$ [#] [10 ⁹ cm]	L_{Reale} ^{**} [10 ⁹ cm]	τ_{SXR} ^{††} [sec]	ζ ^{‡‡}
2014/12/04-08:03	M1.3	S24W27	12.9	0.8	51.5	65.3	65.5	2.2	5.3	2.4	—	—	—
2014/12/19-09:44	M1.3	S19W27	12.6	0.8	48.8	42.6	27.3	2.4	4.0	2.3	1.1	1144	0.39
2014/12/20-00:28	X1.8	S21W24	18.0	8.9	55.1	89.9	105.9	5.8	8.6	4.6	—	2975	—

*Locations where flares occurred.

[†]Temperature in unit 10⁶K when emission measure is maximum value.[‡]Emission measure in unit 10⁴⁸ cm⁻³.[§]Theoretically estimated physical quantities by Shibata & Yokoyama (2002).^{||}Observationally measured physical quantities in the case of (a).[#]Observationally measured physical quantities in the case of (b).^{**}Theoretically estimated loop length by Reale et al. (1997).^{††}Flare duration defined as e-folding decay time of soft X-ray intensity.^{‡‡}The trajectory of $\sqrt{EM} - T$ diagram.